ORIGINAL ARTICLE

Virtual antenna array for reduced energy per bit transmission at Sub-5 GHz mobile wireless communication systems

Mohammad Alibakhshikenari [a], Bal Virdee [b], Dion Mariyanayagam [b], Ignacio Garcia Zuazola [b], Haralambos Harry Benetatos [b], Ayman A. Althuwayb [c], Bader Alali [c,d], Kai-Da Xu [e], Francisco Falcone [f,g]

[a] *Department of the Signal Theory and Communications, Universidad Carlos III de Madrid, 28911 Leganés, Madrid, Spain*
[b] *Center for Communications Technology, London Metropolitan University, London, UK*
[c] *Electrical Engineering Department, College of Engineering, Jouf University, Sakaka, Aljouf 72388, Saudi Arabia*
[d] *Center for Wireless Communications, Institute of Electronic, Communications and Information Technology, Queen's University Belfast, Belfast BT3 9DT, Northern Ireland, United Kingdom*
[e] *School of Information and Communications Engineering, Xi'an Jiaotong University, Xi'an 710049, China*
[f] *Department of Electric, Electronic and Communication Engineering and the Institute of Smart Cities, Public University of Navarre, 31006 Pamplona, Spain*
[g] *School of Engineering and Sciences, Tecnologico de Monterrey, Monterrey 64849, Mexico*

Abstract This paper presents an innovative technique to synthesize a virtual antenna array (VAA) that consumes less energy than conventional antenna arrays that are used in mobile communications systems. We have shown that for a specific spectral efficiency a wireless system using the proposed virtual antenna array consumes significantly less energy per bit ($\sim$3 dB) than a wireless system using a conventional multiple-input multiple-output (MIMO) array. This means the adoption of the proposed VAA technology in smartphones, iPad, Tablets and even base-stations should significantly reduce the carbon footprint of wireless systems. The proposed VAA is realized by employing a pair of linear antenna arrays that are placed in an orthogonal configuration relative to each other. This orthogonal arrangement ensures the radiation is circularly polarized. The size of the standard radiating elements constituting the VAA were miniaturized using the topology optimization method. The design of the VAA incorporates substrate integrated waveguide (SIW) and metasurface technologies. The function of SIW in the design was twofold, namely, to reduce energy loss in the substrate on which the VAA is implemented, and secondly to mitigate unwanted electromagnetic interactions between the neighboring radiating elements and thereby enhancing isolation which otherwise would degrade the radiation characteristics of the array. Metasurface technology

served to effectively increase the effective aperture of the array with no impact on the footprint of the array. The consequence of SIW and metasurface technologies was improvement in the gain and radiation efficiency of the array. The proposed four orthogonal 4-element VAA covers the entire sub-5 GHz frequency range, and it radiates bidirectional in the azimuth plane and omnidirectional in the elevation plane. Moreover, it is relatively easy to design and fabricate. The proposed VAA has dimensions of $0.96\lambda_0 \times 0.96\lambda_0 \times 0.0016\lambda_0$ at mid-band frequency of 3 GHz. VAA has a measured gain of 25 dBi and radiates with 90% efficiency. The average isolation between the linear arrays constituting the virtual array is better than 27 dB.

1. Introduction

THE mobile industry recognizes the global climate crisis is a formidable challenge and it has contributed to this crisis with the growth in mobile traffic over the past decade by a factor of almost 300 [1]. However, mobile service providers have accommodated the expansion of this traffic by consuming just 64% of energy, i.e., globally 150 Terawatt-hour (TWh) [2]. This has been made possible with the recent technological advancements. Nevertheless, mobile networks consume a considerable amount of energy.

Bit-per-joule energy efficiency is an important design metric for 5G wireless networks. The key enabler in achieving this energy efficiency is massive multiple input multiple output (MIMO) technology [3,4]. With massive MIMO the base-stations are furnished with numerous radiating elements which is necessary to realize significant improvement in spectral and energy efficiency over 4G long-term evolution (LTE) networks. Massive MIMO in 5G directs base-station energy to the users, which brings drastic improvements in throughput and efficiency. With this technology 3D beamforming makes possible dynamic coverage required for users traveling in vehicles and it appropriately adjusts the transmission towards the user's location. However, by increasing the size of the MIMO system does not necessarily translate to enhancement in energy efficiency, because the power consumption by the MIMO system also proportionately increases [5].

As 5G is scaled up to satisfy consumer and industry appetite for new and improved services the energy stakes are expected to get even higher. By 2025 the mobile traffic is expected to quadruple. The implication of this is a significant increase in the energy consumption by wireless mobile networks. The challenge is how to reduce the energy without negatively impacting on the system's performance. Service providers have begun to integrate artificial intelligence (AI) into mobile networks. AI is leveraged to optimize network performance including energy efficiency. Moreover, service providers are applying power-saving solutions using machine learning techniques without blocking the cells. This is done by monitor the traffic flow, i.e., data volume and users, across the whole network.

Another strategy to reduce energy consumption of mobile systems is by employing MIMO in 5G mobile handsets thus enabling energy to be focused to the base-station instead of radiating it omnidirectionally. Several MIMO 5G smartphone antennas have been reported recently in literature [6–12]. The disadvantage of these antennas is either a narrow impedance bandwidth or the use of a single-polarized uniplanar radiating element. Moreover, most of these antennae do not support sub-5 GHz 5G bands. MIMO system in existing mobile handsets comprise two or four antennas in a single physical package, which makes them less resilient to interference. This issue can be circumvented by using many antennas in the MIMO system, however the issue with accommodating a large number of antennas in a finite space is the detrimental effect of unwanted near-field coupling that can affect the overall performance of the MIMO system.

We believe the solution is to implement the MIMO system with a virtual antenna array (VAA) [13–16]. Compared to traditional antenna arrays (TAA), VAA use fewer radiators to generate a more focused beam pattern as though it was generated from a much larger array. Also, unlike TAA where the size of the array dictates its angular resolution, in VAA the angular resolution is determined by the spatial diversity of the transmit signal. For a large MIMO VAA the angular resolution depends on the bandwidth of the array.

In this paper, the feasibility of low energy MIMO VAA is investigated for future base-stations and smartphone handsets. The prototype of the proposed MIMO VAA consists of orthogonal facing pairs of four triangular shaped radiators arranged in proximity to each other to realize circularly polarized waves. Topology optimization method was used to reduce the size of the triangular patch radiators. The design of the virtual array included substrate integrated waveguide (SIW) and metasurface technologies. Each pair of radiators constituting the array is excited using a network of power dividers. Theoretical analysis reveals the virtual array virtual array consumes significantly less energy per bit than an ideal MIMO. The proposed MIMO VAA was first modelled in a 3D full-wave electromagnetic solver that used finite integration technique to define Maxwell's equations on a grid space in the time and frequency domains. The proposed MIMO VAA is shown to reduce energy loss that results in increased radiation efficiency and gain performance. The proposed technology should contribute towards reducing carbon emissions in wireless communications systems.

2. Virtual antenna array theoritical background

The MIMO VAA can be realized by having a linear antenna array of M radiating elements and N receiving elements that are arranged in an orthogonal plane to each other, as illustrated in Fig. 1. The orientation of the transmit and receive antenna arrays and the inter radiator gap dictate the size of the virtual antenna array. Convolution of the signals at the transmit and the receive antennas results in a resultant signal
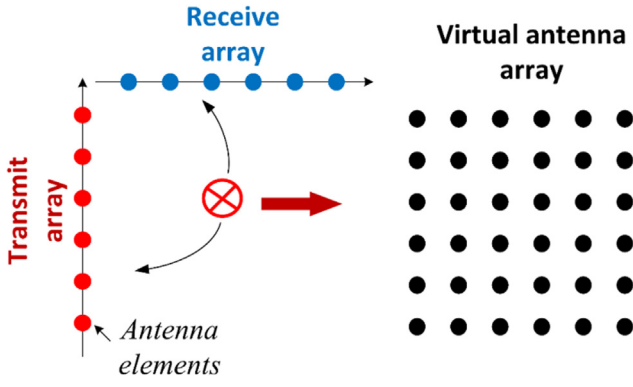
Fig. 1 MIMO virtual antenna array created from orthogonal linear antenna arrays.

that is equivalent to a much larger array having a significantly larger resolution than the constituent linear arrays.

Radiation pattern of the transmit and receive linear arrays can be represented by

$$AP_t(\theta, \varnothing) = \sum_{m=1}^{M} \alpha_{t,m} e^{jkd_t sin\theta cos\varnothing} \tag{1}$$

$$P_r(\theta, \varnothing) = \sum_{n=1}^{N} \alpha_{r,n} e^{jkd_r sin\theta cos\varnothing} \tag{2}$$

where $\alpha_{t,m}$ and $\alpha_{r,n}$ are the complex excitation coefficients of the mth and n^{th} antenna in the transmission and receiver arrays, respectively, d_t is the position vector of the transmit array, d_r is the position vector of the receive array, $k = 2\pi/\lambda_o$, λ_o is the free-space wavelength, and θ and ϕ are the spherical polar and azimuth angles, respectively.

The transmit and receive arrays have a gain that is proportional to the square of the array-factor given by

$$G_t(\theta, \phi) \propto |AP_t(\theta, \varnothing)|^2 \tag{3}$$

$$G_r(\theta, \phi) \propto |AP_r(\theta, \varnothing)|^2 \tag{4}$$

The radiation pattern of the virtual antenna array can be found by taking the Kronecker product of the array pattern of the transmit and receive arrays, which is represented by

$$AP(\theta, \varnothing) = \sum_{m=1}^{M} \alpha_{t,m} e^{jkd_t sin\theta cos\varnothing} \bigotimes \sum_{n=1}^{N} \alpha_{r,n} e^{jkd_r sin\theta cos\varnothing} \tag{5}$$

and the corresponding gain of the virtual array is

$$G(\theta, \varnothing) = G_t(\theta, \phi) \bigotimes G_r(\theta, \phi) \tag{6}$$

The advantage of the virtual array is its ability to reduce the number of radiators but provide the performance of a significantly larger array. A virtual array comprising 12 transmit elements and 12 receive elements has an equivalent radiation pattern of the 144 elements. Moreover, it reduces the complication and the energy losses associated with the excitation feed network.

Expressions for the energy and spectral efficiency can be determined by considering the orthogonal linear antenna arrays in Fig. 1. Let $x = [x_1, x_2]^T$ represent the transmitter vector. The receiver vector $[y_1, y_2]^T$ can be represented by [17]:

$$\begin{bmatrix} y_1 \\ y_2 \end{bmatrix} = Hx + n; H = \begin{bmatrix} d_1 & d_2 \\ d_3 & d_4 \end{bmatrix} \tag{7}$$

where H represents the array matrix and the noise-vector is defined by $n = [n_{v1}, n_{v2}]^T$, where $n_{v1}, n_{v2} \sim \mathscr{CN}(0, N_0)$ are independent and identically distributed zero-mean complex Gaussian noise with $N_0 = 1$ Watts/Hz. With the compress-and-forward (CF) protocol, the array is comparable to a system where the two-antenna receiver intercept the signals $[y_r + n_c, y_d]^T$, where $n_c \sim \mathscr{CN}(0, \sigma_c^2)$ is the compression noise [17]. Using a regular source coding technique, the variance of the compression noise can be expressed as [18]

$$\sigma_c^2 = \frac{\mathbb{E}\left[|y_r|^2\right]}{[1 + GP_r/(N_0 W_r)]^{W_r/W} - 1} = \frac{|d_1|^2 P_{t1} + |d_2|^2 P_{t2} + 1}{GP_r} \tag{8}$$

where P_{t1} and P_{t2} are power applied to the transmit elements, P_r is the total power at the receive elements, and R_c is the coding rate given by

$$R_c = W_r log_2\left[1 + \frac{GP_r}{N_0 W_r}\right] \tag{9}$$

The receiver degrades $y_1 + n_c$ by factor η, such that $\sqrt{\eta}(y_1 + n_c)$, and y_2 have identical additive Gaussian noise, i.e.,

$$\tilde{y} = \left[\sqrt{\eta}(y_1 + n_c), y_2\right]^T = \tilde{H}x + \left[\tilde{n}_1, \tilde{n}_2\right]^T \tag{10}$$

where

$$\tilde{H} \triangleq \begin{bmatrix} \sqrt{\eta}d_1 & \sqrt{\eta}d_2 \\ d_3 & d_4 \end{bmatrix}; \eta \triangleq \frac{1}{1 + \sigma_c^2}$$

and $\tilde{n}_1 \sim$ independent and identically distributed $\mathscr{CN}(0, 1)$. The overall capacity of the system using the C_{CF} protocol is represented by [19]

$$C_{CF} = \mathbb{E}\{log_2 det[I + \tilde{H}(\frac{P_t}{2}I)\tilde{H}^+]\} \tag{11}$$

H^+ denotes the conjugate transpose of H. The energy efficiency is defined as consumption in the transmission energy per information bit [20], i.e., $E_b = P/C_{CF}$, where P is the total consumed power in the system. Because C_{CF} denotes spectral efficiency as a function of E_b, Eqn. (11) can be used to examine the energy efficiency of the virtual antenna array as a function of spectral efficiency however this is a non-trivial problem. It is therefore necessary to use an approximation of Eqn. (11) given by

$$\left.\frac{E_b}{N_0}\right|_{dB} \approx \left.\frac{E_b}{N_{0min}}\right|_{dB} + C_{CF}\frac{10log_{10}2}{S_0} \tag{12}$$

where

$$\frac{E_b}{N_{0min}} = \frac{0.69}{(C_{CF})'_{P=0}}; S_0 = \frac{2.\left[(C_{CF})'_P|_{P=0}\right]^2}{(C_{CF})''_P|_{P=0}}$$

where $(C_{CF})'_P$ and $(C_{CF})''_P$ denote the 1st-order and 2nd-order derivatives of the function C_{CF} with respect to P. Eqn.(12) takes into account Rayleigh fading channels. In low spectral efficiency regime, Eqn.(12) reduces to

$$\left.\frac{E_b}{N_0}\right|_{dB} \approx ln(2)|_{dB} + C_{CF}10log_{10}2 \tag{13}$$

The approximation in Eqn.(13) gives a good insight into the energy efficiency performance as a function of spectral efficiency. This is shown in the simulation results, see Fig. 2, of the energy efficiency performance against spectral efficiency of the virtual antenna array and an ideal MIMO array. The results show that for a specific spectral efficiency the virtual array exhibits a better energy efficiency performance by approximately 3 dB. By adopting VAA technology in smartphone handsets and even base-stations it should significantly reduce the carbon footprint of wireless mobile systems.

3. Virtual antenna array synthesis

The virtual antenna array proposed here is shown in Fig. 3. The antenna was fabricated using LPKF ProtoMat system. The antenna essentially consists of two VAAs where each virtual array is constituted from two orthogonally arranged linear arrays. Each radiation element is a standard triangular shaped patch, and each linear array comprises four pairs of antennas. The physical side length of the equilateral triangular shaped patch antenna is given by $a = 2c/3f_r\sqrt{\varepsilon_{eff}}$, where c is velocity of light in free-space, f_r is the resonance frequency of the antenna, and ε_{eff} is the effective permittivity of the dielectric substrate on which the antenna is constructed in [21]. The patch antenna was miniaturized by 73.6% using the topology optimization method described in [22] and incorporating a metamaterial structure.

The VAA was constructed on TF920 PTFE ceramic composite dielectric substrate with a dielectric constant of 9.2, tan δ of 0.001, and thickness of 0.8 mm. The proposed VAA has dimensions $198.98 \times 198.9 \times 1.6$ mm^3. The orthogonal pair of linear arrays made of eight antennas is equivalent to a standard MIMO array consisting of 64 elements. The orthogonal arrangement of linear arrays makes it possible to include another pair of orthogonal linear arrays as shown in Fig. 1. This dual VAA arrangement not only improves the gain performance and the radiation pattern of the VAA but when located on the smartphone handset it ensures the antennas are not obscured completely by the user's hands which is important to ensure communication is reliable. Also, shown
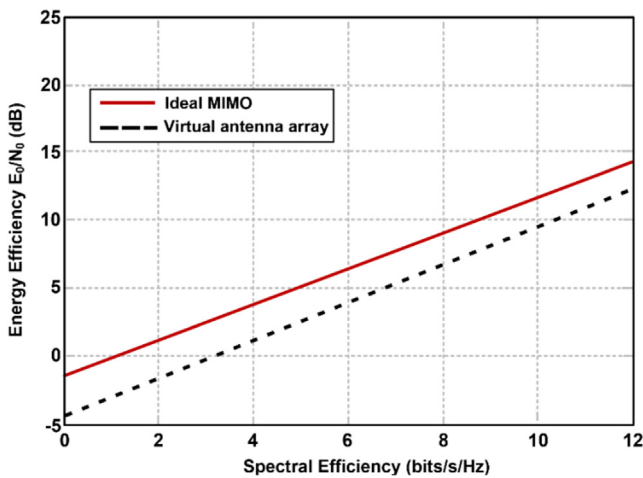

Fig. 2 Energy efficiency of the virtual antenna array compared with an ideal MIMO array.
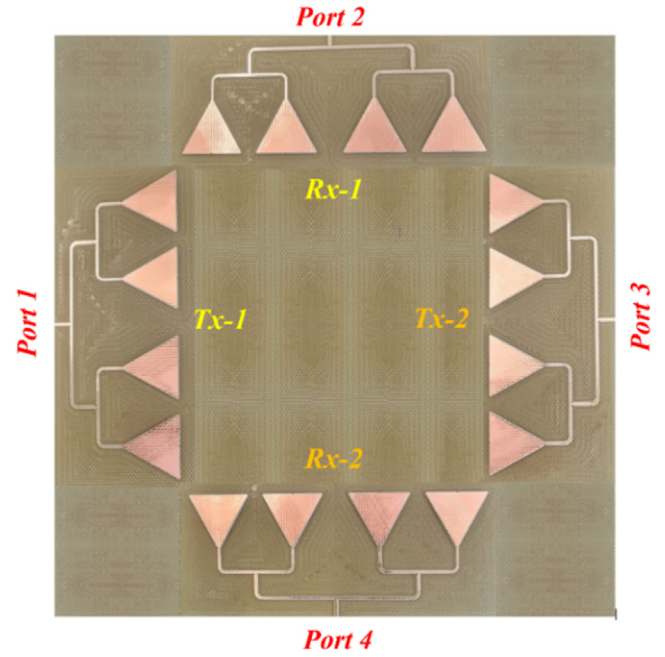

Fig. 3 Dual virtual antenna array (VAA) of orthogonal transmit and receive linear arrays.

in Fig. 3 is the feed mechanism which consists of a network of Wilkinson power dividers. The feed network is designed to assure phase coherence is maintained at the radiators. The gap between the radiation elements was optimized for gain and efficiency performance using a commercial 3D full-wave electromagnetic solver based on finite integration technique. The underside of the substrate on which the VAA is designed is a ground-plane.

The radiation characteristics of the fabricated VAA was measured in a standard anechoic chamber using the set-up shown in Fig. 4. The antenna was fed RF energy through SMA connectors. The transmit and receive arrays were connected to the vector network analyzer. The measured S-parameter responses of the proposed VAA is shown in Fig. 5. The reflection coefficient (S$_{11}$) shows that the virtual array operates between 1.08–2.02 GHz, 2.96–3.36 GHz, 3.76–4.12 GHz, and 4.86–5 GHz for $|S_{11}| \leq$ -10 dB. The isolation between the adjacent arrays over the operating range is better than 10 dB. The antenna gain and radiation efficiency of the VAA are shown in Fig. 6. The gain and efficiency at mid operating range of 1.55 GHz, 3.16 GHz, 3.94 GHz, and 4.93 GHz are 4.1 dBi & 48.8%, 3.4 dBi & 48%, 1.7 dBi & 49%, and 5 dBi & 47.1%, respectively.

Inter-array isolation of the virtual array was improved by employing the concept of substrate integrated-waveguide that involved inserting metallic via-pins between the linear arrays as shown in Fig. 7. The metallic via-pins are also inserted between the patches and around the feed network to reduce energy loss and minimize unwanted mutual coupling caused by surface waves that would otherwise degrade the array's radiation performance. The diameter of the metal posts and the gap between them were determined using expressions in [23].

The S-parameter performance of the VAA with SIW is shown in Fig. 8. The effect of applying SIW on the virtual
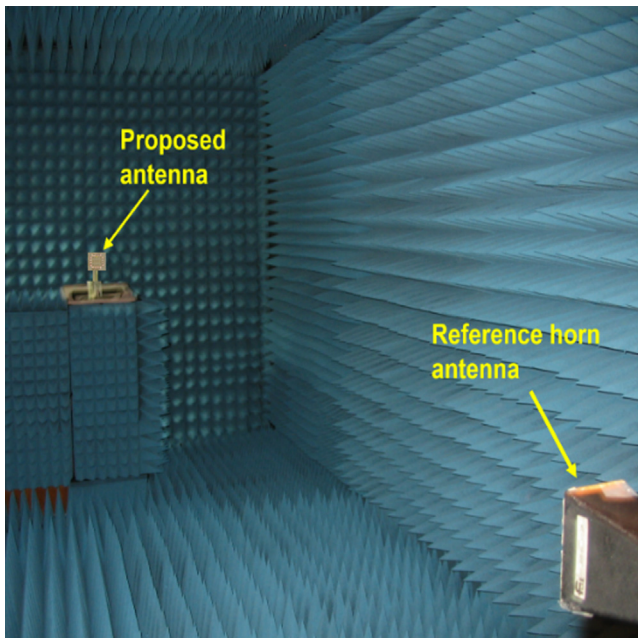
Fig. 4   Antenna measurement setup.

Fig. 7   Layout of the VAA with substrate integrated waveguide (SIW).

Tx-1 & Rx-2 arrays (S_{14}) is better 15 dB than across 1.25–5 GHz.

The effect of SIW on the virtual array's gain and efficiency are shown in Fig. 9. Compared to the basic VAA the gain and efficiency with SIW have improved substantially. The average gain of the basic VAA is 2.5 dBi and with SIW the average
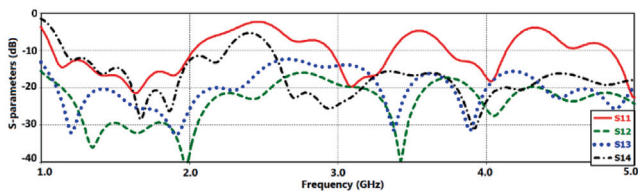

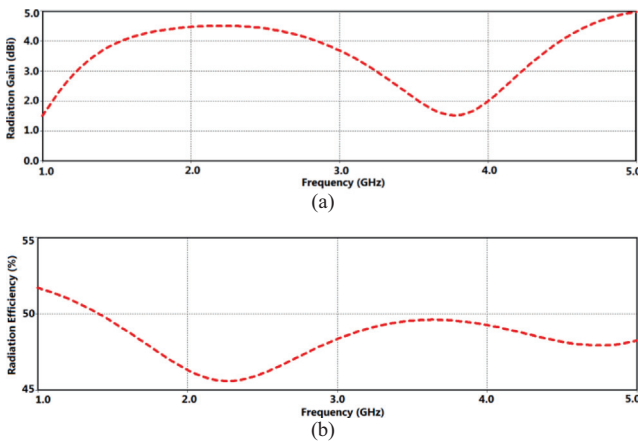Fig. 5   Measured S-parameter responses of the proposed VAA.

Fig. 6   Measured radiation characteristics of the VAA, (a) gain, and (b) efficiency.

array has significantly improved the reflection coefficient and therefore the impedance matching as well as the isolation between the linear arrays. The operational range of the virtual array extends across 1–5 GHz for $|S_{11}| \leq$ -10 dB. The isolation between Tx-1 & Rx-1 arrays (S_{12}) is better than 20 dB across 1–5 GHz. The isolation between Tx-1 & Tx-2 arrays (S_{13}) is better than 20 dB across 1.1–5 GHz, and the isolation between
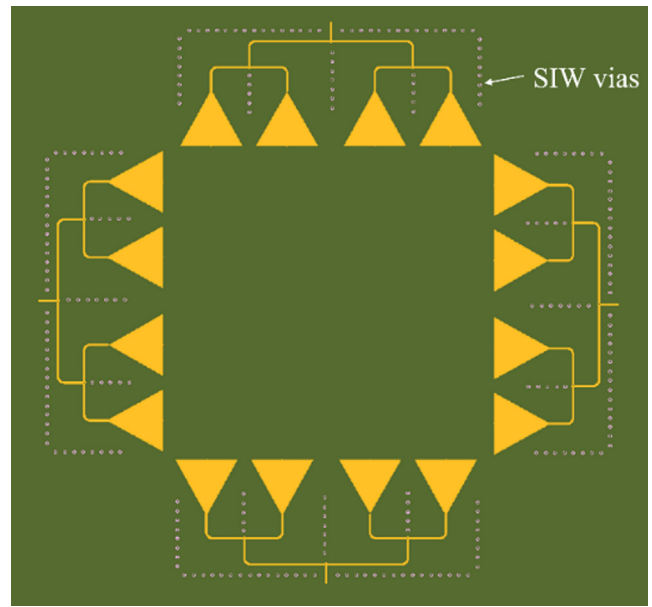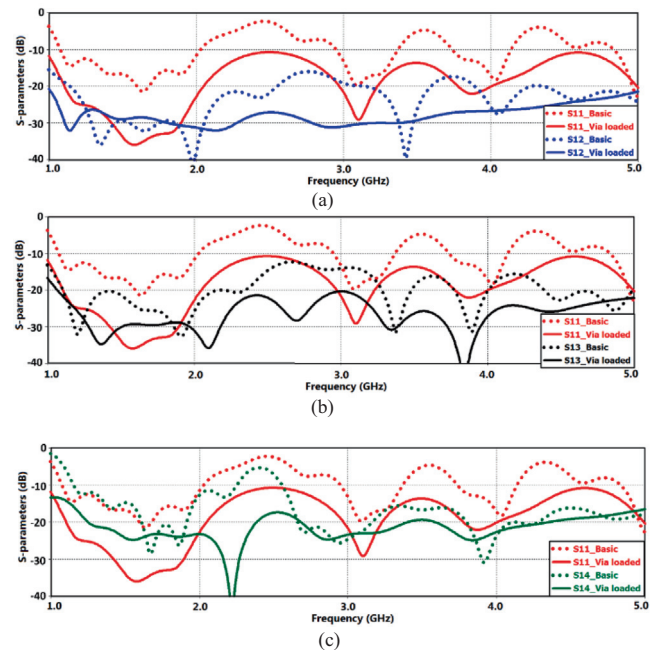

Fig. 8   S-parameter responses of the proposed VAA without and with SIW, (a) reflection coefficient (S_{11}) and isolation between Tx-1 & Rx-1 arrays (S_{12}), (b) reflection coefficient (S_{11}) and isolation between Tx-1 & Tx-2 arrays (S_{13}), and (c) reflection coefficient (S_{11}) and isolation between Tx-1 & Rx-2 arrays (S_{14}).
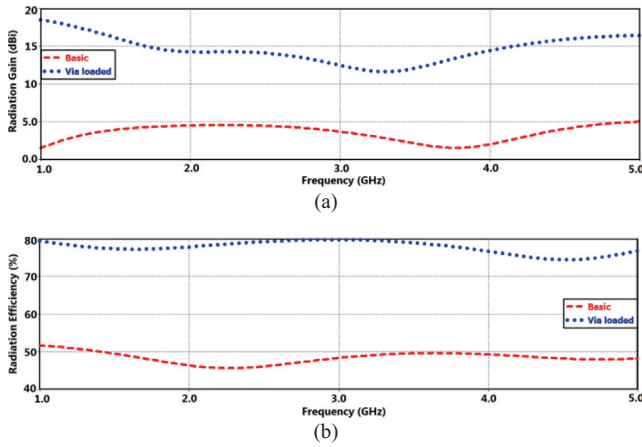
Fig. 9   The VAA with SIW, (a) gain, and (b) efficiency.

gain is 15 dBi, which constitutes gain improvement of 12.5 dB. Similarly, the average efficiency of the basic VAA is 48%, and with SIW the average efficiency jumps to 78%, which is an improvement in efficiency of 30%. These results demonstrate the effectiveness of using SIW.

Further reduction in the physical size of the patch antenna can be achieved by transforming the patch antenna into a metamaterial surface. This can be achieved by embedding two concentric split ring slots in the patch antenna where the slits are located 180 degrees apart as shown in Fig. 10. The slot gap in the rings acts as a distributed capacitance, while the metallization ring between the split ring slots acts as an inductor. The equivalent circuit model of the complementary split ring (CSRR) is shown in Fig. 11 where the capacitive coupling and inductive coupling between two rings are modeled by a coupling capacitance (C_m) and by a transformer, respectively. When the rings are excited by a time varying signal the combination of the two rings acts as an LC resonance circuit. Dimensions of the proposed VAA are given in Table 1.

The complementary slit ring resonator exhibits a negative effective permittivity in the vicinity of the fundamental CSRR resonance. The effective permeability of CSRR is given by [24]

$$\mu_{eff} = \mu'_{eff} - j\mu'_{eff} = 1 - \frac{f_{mp}^2 - f_0^2}{f^2 - f_0^2 - j\gamma f} \tag{14}$$

where f is the frequency of the signal, f_{mp} is the frequency at which $\mu_{eff} = 0$, f_0 is the frequency at which μ_{eff} diverges, and γ represents the loss. It is shown in [25] that by applying metamaterial characteristics to the patch its size can be reduced by 42% and its bandwidth increased by 41%.

Fig. 12 shows the S-parameter responses of the proposed VAA with SIW and loaded with metasurface are compared with the basic virtual array and the virtual array with SIW vias. Compared to the previous iterations Fig. 12(a) shows the virtual array loaded with metasurface provides a superior impedance match across 1–5 GHz for $|S_{11}| \leq$ -10 dB. In fact, the average reflection coefficient is better than −20 dB. Fig. 12(b)-(d) shows the isolation too is superior between the linear arrays of the virtual array loaded with metasurface. The average isolation between Tx-1 & Rx-1 arrays (S_{12}) is better than 30 dB, between Tx-1 & Tx-2 arrays (S_{13}) is better than 40 dB, and between Tx-1 & Rx-2 arrays (S_{14}) is better than 27 dB.
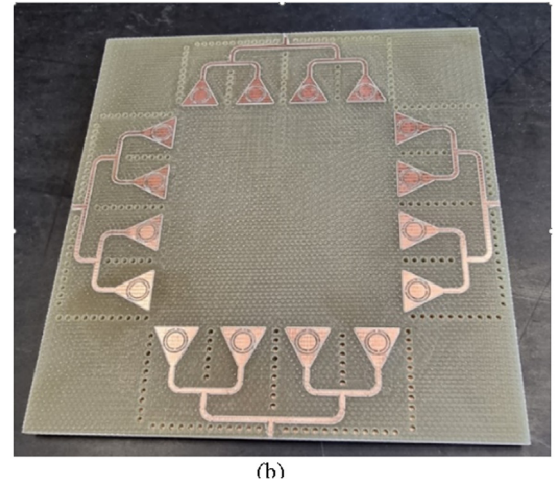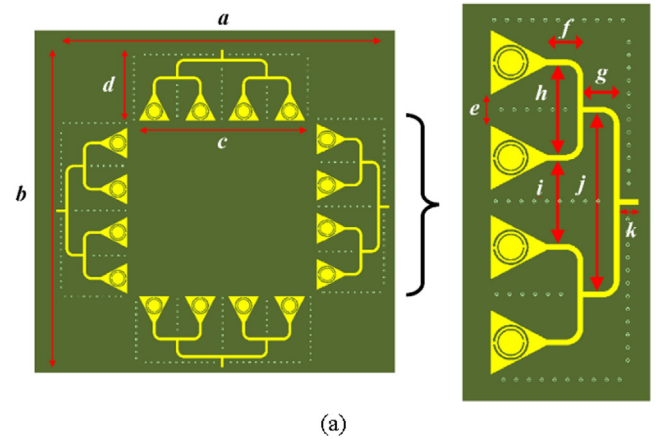

(a)

(b)

Fig. 10   The VAA with SIW and metamaterial CSRR, (a) Layout, and (b) Fabricated prototype.
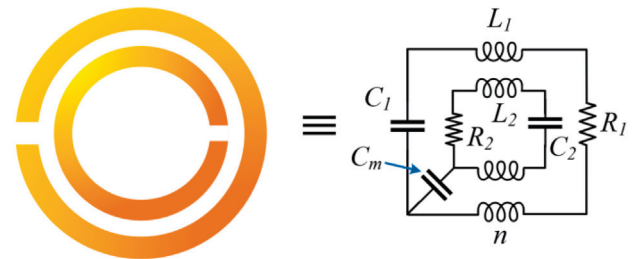

Fig. 11   Equivalent circuit model of the split ring resonator.

The radiation characteristics of the VAA iterations are compared in Fig. 13. It is evident from these results that the virtual array that incorporates a combination of SIW and metasurface provides superior gain and efficiency performance compared to the basic VAA. In fact, across 1–5 GHz the average gain is improves by 21 dBi to 25 dBi, and the efficiency increases by 42% to 90%. The improvement in the array's performance with SIW is due to reduction in the dielectric loss and the high isolation between the adjacent radiators, as evident in Fig. 12, thereby preventing unwanted mutual coupling that would otherwise negatively impact on the array's characteristics. In fact, with SIW the radiators can be tightly arranged thus reducing the array's footprint [26]. The metasur-

Table 1 Geometrical Design Parameters of the VAA.

Parameter	Value (mm)
a	96
b	96
c	48
d	20
e	4.2
f	5
g	5
h	12.6
i	11.8
j	25.3
k	2.8
Patch sides	9
Inner ring radius	1.53
Outer ring radius	2.35
Ring width	68
Ring gap	0.3
Feedline width	0.8
Vias radius	0.2
Vias gap	1.8
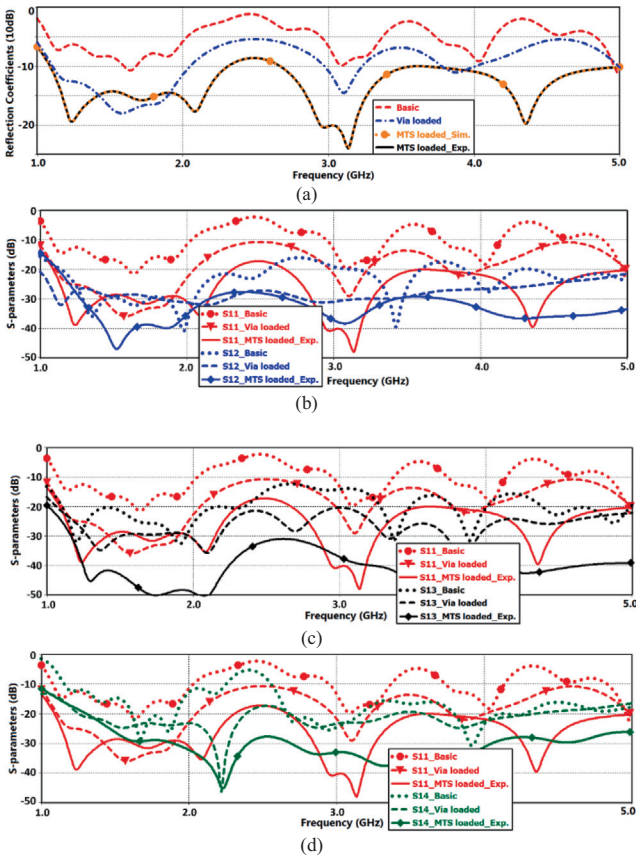
Fig. 12 S-parameter response comparison of the proposed metasurface-based VAA with SIW, VAA loaded with SIW vias, and the basic VAA, (a) reflection coefficient (S$_{11}$) responses, (b) reflection coefficient (S$_{11}$) and isolation between Tx-1 & Rx-1 arrays (S$_{12}$), (c) reflection coefficient (S$_{11}$) and isolation between Tx-1 & Tx-2 arrays (S$_{13}$), and (d) and reflection coefficient (S$_{11}$) and isolation between Tx-1 & Rx-2 arrays (S$_{14}$).
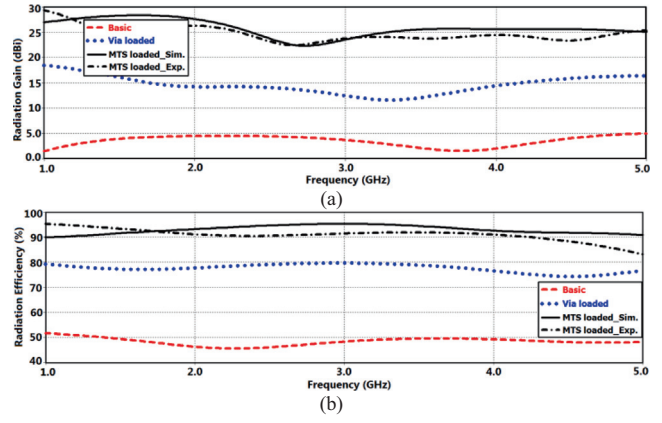
Fig. 13 Comparison of the radiation characteristics of the proposed metasurface-based VAA with SIW, VAA loaded with SIW vias, and the basic VAA, (a) gain, and (b) efficiency.

face essentially enlarges the effective aperture area of the VAA to improve its performances with no impact on the array's physical size. These results are summarized in Table 2.

Envelope correlation coefficient (*ECC*) specifies the correlation among the radiating antenna elements in an antenna array and is defined as [27]

$$ECC = \frac{\left| \iint\limits_{4\pi} E_1(\theta, \phi).E_2^*(\theta, \phi)d\Omega \right|}{\int_{4\pi} E_1(\theta, \phi).E_1^*(\theta, \phi)d\Omega \iint\limits_{4\pi} E_2(\theta, \phi).E_2^*(\theta, \phi)d\Omega} \quad (15)$$

where E_1 and E_2 are far-field radiation patterns, emanating from the two respective ports. Antenna arrays with a low correlation can support high data throughput. *ECC* can be determined from S-parameters measurements using [27]

$$ECC = \frac{\left| S_{11}^* S_{12} + S_{22}^* S_{21} \right|^2}{\left[1 - \left(|S_{11}|^2 + |S_{21}|^2 \right) \right] \left[1 - \left(|S_{22}|^2 + |S_{12}|^2 \right) \right]} \quad (16)$$

The corresponding diversity gain (*DG*) can be determined using

$$DG = 10\sqrt{1 - ECC} \quad (17)$$

In an ideal situation the magnitude of *ECC* should equate to zero. In practical applications, however, an *ECC* < 0.5 is permissible. Fig. 14 show how the measured *ECC* and *DG* vary across the proposed array's frequency range. The correlation is < 0.06 between the antennas in the array, and *DG* is > 9.7 dB. This verifies the diversity of the proposed array is excellent and applicable for high data rate transmission systems.

The radiation patterns of the VAA were measured in a standard anechoic chamber using the set-up shown in Fig. 4. The virtual array was fixed on a platform with rotational facility in the azimuth and elevation planes. Fig. 15 shows the measured radiation patterns of the proposed VAA loaded with both SIW and metasurface. The radiation patterns are shown in the azimuth and elevation planes at spot frequencies within the operating range of the virtual array. The results show the proposed virtual array radiates energy bidirectionally in the azimuth plane and effectively omni-directionally in elevation plane.

Table 2 Comparison of Radiation Characteristics.

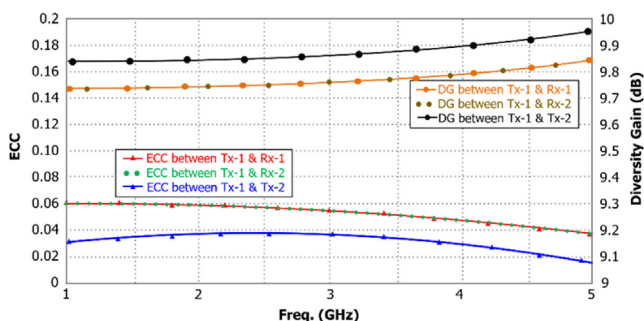|	Basic VAA	VAA loaded with SIW vias	VAA loaded with SIW & MTS	Improvement
Average gain	4 dBi	15 dBi	25 dBi	21 dBi
Average efficiency	48%	78%	90%	42%

Fig. 14 The measured envelop correlation coefficient (*ECC*) and diversity gain (*DG*) of the proposed antenna array.

4. State-of-the-art comparisons

Relevant metrics of the proposed VAA are compared with antenna arrays recently reported in Table 3. Compared to other works cited in the table the proposed virtual antenna array exhibits the widest impedance bandwidth, the largest gain, the second highest radiation efficiency, and the lowest ECC variation. Moreover, the dimensions of the proposed array are much smaller than the arrays cited. These attributes demonstrate the viability of the proposed virtual antenna array for wireless mobile applications.

5. Conclusion

The feasibility of the proposed virtual antenna array is shown to be viable for low energy consumption wireless communications systems. The adoption of this innovative technology should greatly contribute to reduction of greenhouse gases that can adversely impact the global climate. Although in this study the size of the VAA is applicable for mobile handsets however the design can be used to implement massive MIMO in base-stations. The design of the proposed virtual array amalgamates various techniques and technologies. This was necessary to (i) shrink the physical size of the array, (ii) reduce energy loss and thereby enhance the array's radiation characteristics, (iii) mitigated mutual coupling between radiators that can otherwise degrade the radiation characteristics of the array, and (iv) increase the arrays aperture size without affecting the array's size. The proposed 16-element array is shown to operate across the entire sub-5 GHz frequency range, and radiate energy bidirectional in the azimuth plane and omni-directional in the elevation plane. The VAA is shown to have a measured gain of 25 dBi and radiation efficiency of 90%. The average isolation between the linear arrays forming the VAA is better than 27 dB.
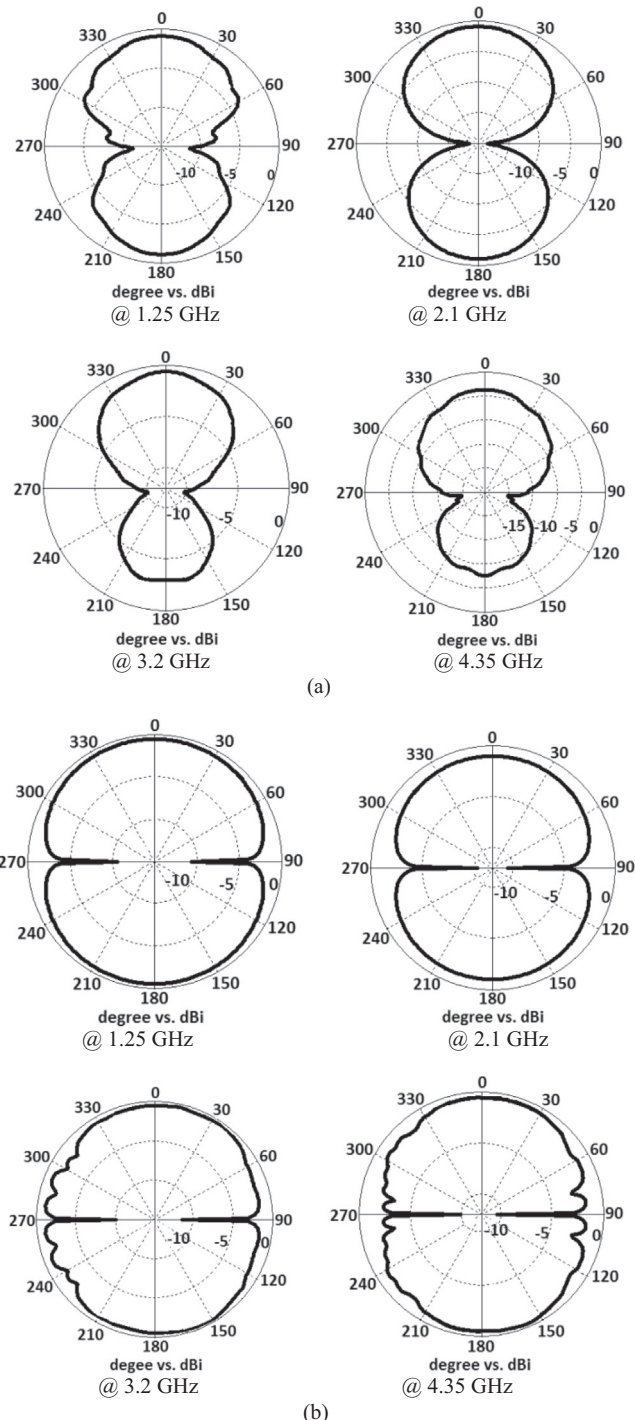

Fig. 15 Measured radiation patterns of the VAA loaded with both SIW and metasurface in (a) azimuth plane, and (b) elevation plane at spot frequencies of 1.25 GHz, 2.1 GHz, 3.2 GHz, and 4.35 GHz.

Table 3 Performance Comparison Between the Proposed VAA and Other State-of-the-Art Antenna Arrays.

Ref.	Antenna layout	ε_r	Size $(\lambda_o)^2$	Imp. BW (GHz)	Center freq. (GHz)	Gain (dBi)	Eff. (%)	ECC (%)
[28]	Reflectarray and patch	3.55	1.82 × 1.82	0.5	3.5	13.7	74	–
[29]	Planar array (4 × 4)	2.97	2 × 2	0.5	5.6	11.5	65	–
[30]	Ground surrounded patch/slot (8 × 8)	2.2	1.55 × 1.35	0.17	3.6	10.9	72.8	–
[31]	Dual-feed patch (2 × 2)	2.5	4 × 4	0.8	9.4	4.51	–	–
[32]	Slot MIMO	2.2	0.65 × 1.34	0.6/ 0.2	1.9/ 2.6	3.25/ 6.5	65/ 70	14–4
[33]	Circle-slotted parasitic (8 × 8)	2.17	4.5 × 4.95	1.5	5.3	18.9	30.6	–
[34]	Nonuniform array	3.5	10.12 × 10.12	0.36	25.3	12	–	–
[35]	MIMO using metamaterial mushroom (1 × 8)	3.5	0.96 × 0.96	0.054	2.4	4	–	8–1
[36]	Dielectric Resonator MIMO (1 × 2)	9.8	1.33 × 0.97	0.34	4	4	93	10–3
This Work	SIW + Metasurface (4 × 4) Rx, (4 × 4) Tx	4.3	0.96 × 0.96	4	3	25	90	6–1.8

Declaration of Competing Interest

Acknowledgments

References

[1] Ericsson Mobility Report, November 2021. www.ericsson.com/mobility-report.

[2] Mobile Net Zero, State of the Industry on Climate Action 2021, www.gsma.com.

[3] M.A. Abu-Rgheff, 5G Physical Layer Technologies, September 2019 Wiley-IEEE Press, ISBN: 978-1-119-52549-3.

[4] Y.J. Guo, R.W. Ziolkowski (Editors), Antenna and Array Technologies for Future Wireless Ecosystems, Wiley, August 2022. ISBN: 978-1-119-81388-0.

[5] K.N.R.S.V. Prasad, E. Hossain, V.K. Bhargava, Energy efficiency in massive MIMO-based 5G networks: opportunities and challenges, IEEE Wireless Commun. (2017) 86–94.

[6] X. Zhao, S.P. Yeo, L.C. Ong L.C, Decoupling of inverted-F antennas with high-order modes of ground plane for 5G mobile MIMO platform, IEEE Trans. Antennas Propag. 66 (2018) 4485–4495.

[7] N.O. Parchin, Y.I. Al-Yasir, H.J. Basherlou, R.A. Abd-Alhameed, J.M. Noras, Orthogonally dual-polarised MIMO antenna array with pattern diversity for use in 5G smartphones, IET Microw. Antennas Propag. 14 (6) (2020) 457–467.

[8] A. Zhao, R. Zhouyou, Size reduction of self-isolated MIMO antenna system for 5G mobile phone applications, IEEE Antennas Wirel. Propag. Lett. 18 (2019) 152–156.

[9] X. Zhang, Y. Li, W. Wang, W. Shen, Ultra-wideband 8-port MIMO antenna array for 5G metal-frame smartphones, IEEE Access 7 (2019) 72273–72282.

[10] A. Zhao, Z. Ren, Wideband MIMO antenna systems based on coupled-loop antenna for 5G N77/N78/N79 applications in mobile terminals, IEEE Access 7 (2019) 93761–93771.

[11] D.Q. Liu, H.J. Luo, M. Zhang, H.L. Wen, B. Wang, J. Wang, An extremely low-profile wideband MIMO antenna for 5G smart-phones, IEEE Trans. Antennas Propag. 67 (2019) 5772–5780.

[12] Z. Ji et al, Low mutual coupling design for 5G MIMO antennas using multi-feed technology and its application on metal-rimmed mobile phones, IEEE Access 9 (2021) 151023–151036.

[13] W.-Q. Wang, Virtual antenna array analysis for MIMO synthetic aperture radars, Int. J. Antennas Propag. (2012) 1–10.

[14] M. Li, F. Zhang, Y. Ji, W. Fan, Virtual antenna array with directional antennas for millimeter-wave channel characterization, IEEE Trans. Antennas Propag. 70 (8) (Aug. 2022) 6992–7003.

[15] H.S. Dawood, H.A. El-Khobby, M.M.A. Elnaby, A.H. Hussein, Optimized VAA based synthesis of elliptical cylindrical antenna array for SLL reduction and beam thinning using minimum number of elements, IEEE Access 9 (2021) 50949–50960.

[16] J. Cheng, K. Guan, F. Quitin, Direction-of-arrival estimation with virtual antenna array: observability analysis, local oscillator frequency offset compensation, and experimental results, IEEE Trans. Instrum. Meas. 70 (2021) 1–13.

[17] S. Verdu, Spectral efficiency in the wideband regime, IEEE Trans. Inform. Theory 48 (6) (Jun. 2002) 1319–1343.

[18] T.T. Kim, M. Skoglund, G. Caire, Quantifying the loss of compress-forward relaying without Wyner-Ziv coding, IEEE Trans. Inform. Theory 55 (4) (2009) 1529–1533.

[19] J. Jiang, J.S. Thompson, P.M. Grant, Design and analysis of compress-and-forward cooperation in a virtual-MIMO detection system, IEEE GLOBECOM Workshop on HeterWMN, Miami, USA, Dec. 2010, pp. 126–130.

[20] J. Gomez-Vilardebo, A. Perez-neira, M. Najar, Energy efficient communications over the AWGN relay channel, IEEE Trans. Wireless Commun. 9 (1) (Jan. 2010) 32–37.

[21] K. Esselle Nasimuddin, A.K. Verma, Resonance frequency of an equalateral triangular microstrip antenna, Microw. Opt. Technol. Lett. 47 (5) (2005) 485–489.

[22] R.A.H. Mahdi, S.M.R. Taha, Miniaturization of rectangular microstrip patch antenna using topology optimized metamaterial, IEICE Electronics Epress 14 (19) (2017) 1–9.

[23] E. Sandi, A. Diamah, M.W. Iqbal, D.N. Fajriah, Design of substrate integrated waveguide to improve antenna performances for 5G mobile communication application, Journal of Physics: Conf. Ser. 1402, 044032, pp. 1-5.

[24] D.R. Smith, J.B. Pendry, M.C.K. Wiltshire, Metamaterials and negative refractive index, Science 305 (5685) (2004) 788–792.

[25] W.J. Krzysztofik, T.N. Cao, Metamaterials in applicaton to improve antenna parameters," Intech Open, Ch.4, 2018. DOI: 10.5772/intechopen.80636.

[26] M. Bozzi, A. Georgiadis, K. Wu, Review of substrate-integrated waveguide circuits and antennas, IET Microwaves Antennas Propag. 5 (8) (2011) 909–920.

[27] S.-H. Kim, J.Y. Chung, Analysis of the envelope correlation coefficient of MIMO antennas connected with suspended lines, J. Electromagn. Eng. Sci. 20 (2) (2020) 83–90.

[28] D.E. Serup, G.F. Pedersen, S. Zhang, Dual-band shared aperture reflectarray and patch antenna array for S- and Ka-bands, IEEE Trans. Antennas Propagation 70 (3) (2022) 2340–2345.

[29] J. Wu, C. Wang, Y.X. Guo, Dual-band co-aperture planar array antenna constituted of segmented patches, IEEE Antennas Wirel. Propag. Lett. 19 (2) (2020) 257–261.

[30] Z.-X. Xia, K.W. Leung, N. Yang, K. Lu, Compact dual-frequency antenna array with large frequency ratio, IEEE Trans. Antennas Propag. 69 (4) (2021) 2031–2040.

[31] K.-B. Kim, B.C. Jung, J.-M. Woo, Compact dual-polarized (CP, LP) with dual-feed microstrip patch array for target detection, IEEE Antennas Wireless Propag. Lett. 19 (4) (2020) 517–521.

[32] S.P. Biswal, S.K. Sharma, S. Das, Collocated microstrip slot MIMO antennas for cellular bands along with 5G phased array antenna for user equipments (UEs), IEEE Access 8 (2020) 209138–209152.

[33] C.E. Santosa, J.T.S. Sumantyo, S. Gao, K. Ito, Broadband circularly polarized microstrip array antenna with curved-truncation and circle-slotted parasitic, IEEE Trans. Antennas Propag. 69 (9) (Sept. 2021) 5524–5533.

[34] A.R. Gutierrez, A. Reyna, L.I. Balderas, M.A. Panduro, A.L. Mendez, Nonuniform antenna array with nonsymmetric feeding network for 5G applications, IEEE Antennas Wirel. Propag. Lett. 21 (2) (Feb. 2022) 346–350.

[35] G. Zhai, Z.N. Chen, X. Qing, Enhanced isolation of a closely spaced four-element MIMO antenna system using metamaterial mushroom, IEEE Antennas Wirel. Propag. Lett. 63 (8) (Aug. 2015) 3362–3370.

[36] A.K. Dwivedi, A. Sharma, A.K. Singh, V. Singh, Metamaterial inspired dielectric resonator MIMO antenna for isolation enhancement and linear to circular polarization of waves, Measurement 182 (109781) (Sept. 2021) 1–12.

Mohammad Alibakhshikenari (Member, IEEE) was born in Mazandaran, Iran, in February 1988. He received the Ph.D. degree (Hons.) with European Label in electronics engineering from the University of Rome "Tor Vergata", Italy, in February 2020. He was a Ph.D. Visiting Researcher at the Chalmers University of Technology, Sweden, in 2018. His training during the Ph.D. included a research stage in the Swedish company Gap Waves AB. He is currently with the Department of Signal Theory and Communications, Universidad Carlos III de Madrid (uc3m), Spain, as the Principal Investigator of the CONEX (CONnecting EXcellence)-Plus Talent Training Program and Marie Skłodowska-Curie Actions. He was also a Lecturer of the electromagnetic fields and electromagnetic laboratory with the Department of Signal Theory and Communications for academic year 2021–2022 and he received the "Teaching Excellent Acknowledgement" Certificate for the course of electromagnetic fields from Vice-Rector of studies of uc3m. Now he is spending an industrial research period in SARAS Technology Limited Company, located in Leeds, United Kingdom, which is defined as his secondment plan by CONEX-Plus Program and Marie Skłodowska-Curie Actions. His research interests include electromagnetic systems, antennas and wave-propagations, metamaterials and metasurfaces, synthetic aperture radars (SAR), 5G and beyond wireless communications, multiple input multiple output (MIMO) systems, RFID tag antennas, substrate integrated waveguides (SIWs), impedance matching circuits, microwave components, millimeter-waves and terahertz integrated circuits, gap waveguide technology, beamforming matrix, and reconfigurable intelligent surfaces (RIS), which led to achieve more than 4500 citations and H-index 43 reported by Google Scholar, and more than 3800 citations and H-index 40 reported by Scopus. He was a recipient of the three years research grant funded by Universidad Carlos III de Madrid and the European Union's Horizon 2020 Research and Innovation Program under the Marie Skłodowska-Curie Grant started in July 2021, the two years research grant funded by the University of Rome "Tor Vergata" started in November 2019, the three years Ph.D. Scholarship funded by the University of Rome "Tor Vergata" started in November 2016, and the two Young Engineer Awards of the 47th and 48th European Microwave Conference were held in Nuremberg, Germany, in 2017, and in Madrid, Spain, in 2018, respectively. His research article entitled "High-Gain Metasurface in Polyimide On-Chip Antenna Based on CRLH-TL for Sub Terahertz Integrated Circuits" published in Scientific Reports was awarded as the Best Month Paper at the University of Bradford, U.K., in April 2020. He is serving as an Associate Editor for (i) Radio Science, and (ii) IET Journal of Engineering. He also acts as a referee in several highly reputed journals and international conferences.

Bal S. Virdee (SM'08) received the B.Sc. and MPhil degrees in Communications-Engineering from the University of Leeds-UK and his Ph.D. in Electronic-Engineering from the University of London-UK. He has worked in industry for various companies including Philips (UK) as an R&D-engineer and Filtronic-Components Ltd. as a future products developer in the area of RF/microwave communications. He has taught at several academic institutions before joining London Metropolitan University where he is a Professor of Microwave-Communications in the Faculty of Life Sciences&Computing where he Heads the Center for Communications-Technology and is the Director of London Metropolitan-Microwaves. His research, in collaboration with industry and academia, is in the area of microwave wireless communications encompassing mobile-phones to satellite-technology. Prof. Virdee has chaired technical sessions at IEEE international conferences and published numerous research-papers. He is Executive-Member of IET's Technical and Professional Network Committee on RF/Microwave-Technology. He is a Fellow of IET and a Senior-Member of IEEE.

Dion Mariyanayagam is experienced Engineer with a demonstrated history of experience in Prototype Development from CAD to embedded programming for Systems Engineering. High administrative professional Graduated with a Bachelor of Engineering (BEng) focused on Computer Systems Engineering from London Metropolitan University (LMU) with a First Class. Currently he is a PhD research student at LMU with a focus on lightweight polymorphic security systems for IoT devices.

Ignacio J. Garcia Zuazola: received the FPII degree in Industrial Electronics from the School of Chemistry and Electronics, Indautxu, Spain, in 1995, the Higher National Diploma in Telecommunications Engineering from the University of Middlesex, London, U.K., in 2000, the B.Eng. degree in Telecommunications Engineering from Queen Mary University of London, in 2003, the Ph.D. degree in Electronics from the University of Kent, Canterbury, U.K., in 2010, and the e-MBA in Business from Cardiff Metropolitan University, Cardiff, U.K., in 2016. He worked at Babcok and Wilcox, Bilbao, Spain in 1993, Iberdrola, Santurce, Spain, in 1995, Telefonica, Bilbao, in 1997, Thyssen Elevators, Bilbao, in 1998, and Cell Communications, Bilbao, in 2000, and engaged in an SME in electrical wiring at Gartzola, Bilbao, in 1996. He was formerly employed as a Research Associate with the University of Kent in 2004 and 2008, a Research Engineer with the University of Wales, Swansea, U.K., in 2006, a Senior Research Fellow with the University of Deusto, Bilbao, in 2011, a Visiting Senior Research Fellow with the University of Leeds, Leeds, U.K., in 2011, and a Research Associate with Loughborough University, Loughborough, U.K., in 2014. He has been a Representative of Spain since 2015 with the London School of Commerce, U.K., and a Research Collaborator with the University of Deusto, Bizkaia, Spain, since 2015. He joined London Metropolitan University as a Senior Lecturer in 2022. Dr Zuazola research interests include business development on one hand and single-band and multiband miniature antennas, and the use of electromagnetic bandgap structures and frequency-selective surfaces. Dr. Zuazola was a recipient of various awards in electrical wiring, pneumatic and hydraulic systems, and robotics.

Harry Benetatos is a senior lecturer in the School of Computing and Digital Media and also acts as course leader for Computer Networking and Cyber Security MSc. Harry holds an MSc in Internet Technology and a BSc (Hons) in Electronic and Communications Engineering. He is a Cisco instructor for CCNA, CCNP, Fundamentals of Network Security, IT Essentials I and II. His areas of expertise are in peer-to-peer networking, distance learning, IT security, and computer networking.

Ayman Abdulhadi Althuwayb received the B. Sc. degree (Hons.) in electrical engineering (electronics and communications) from Jouf University, Saudi Arabia, in 2011, the M.Sc. degree in electrical engineering from California State University, Fullerton, CA, USA, in 2015, and the Ph.D. degree in electrical engineering from Southern Methodist University, Dallas, TX, USA, in 2018. He is currently an Assistant Professor with the department of electrical engineering at Jouf University, Kingdom of Saudi Arabia. His current research interests include antenna design and propagation, microwaves and millimeter-waves, wireless power transfer, ultrawideband and multiband antennas, filters and other.

Bader Alali has received the B. Sc. degree (Hons.) in electrical engineering from Jouf University, Saudi Arabia in 2011 and the M. Sc. degree in electrical engineering from California State University, Fullerton, CA, United States in 2015. Currently, he is a Lecturer at the Department of Electrical Engineering, Jouf University and pursuing the Ph. D. degree with the Institute of Electronic, Communications and Information Technology, Queen's University Belfast, Belfast, Northern Ireland, United Kingdom. His current research interests include millimeter-wave and microwave components and circuits, lens antennas, reflectarray antennas, and electromagnetic field theory.
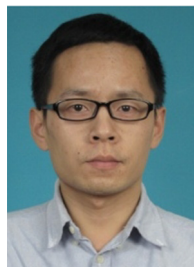
Kai-Da Xu (S'13-M'15-SM'18) received the B. E. and Ph.D. degrees in electromagnetic field and microwave technology from University of Electronic Science and Technology of China (UESTC), Chengdu, China, in 2009 and 2015, respectively. From 2012 to 2014, he was a Visiting Researcher with the Department of Electrical and Computer Engineering, Duke University, Durham, NC, USA, under the financial support from the China Scholarship Council. In 2015, he joined the Department of Electronic Science, Xiamen University, Xiamen, China, as an Assistant Professor. From 2016 to 2017, he was a Postdoctoral Fellow with the State Key Laboratory of Millimeter Waves, City University of Hong Kong, Hong Kong. From 2018 to 2019, he was an Honorary Fellow with the Department of Electrical and Computer Engineering, University of Wisconsin–Madison, WI, USA. He was successfully selected into the "Youth Talent Support Program" of Xi'an Jiaotong University (XJTU) in May 2019, and joined the School of Information and Communications Engineering in XJTU in January 2020. Also, he was awarded a fellowship from the Japan Society for the Promotion of Science (JSPS) and was the JSPS Fellow with the Department of Communications Engineering, Graduate School of Engineering, Tohoku University from November 2019 to May 2021. He has authored and coauthored over 120 papers in peer-reviewed journals and over 40 papers in conference proceedings. His current research interests include RF/microwave, mm-wave/THz devices and antenna arrays. Dr. Xu received the UESTC Outstanding Graduate Awards in 2009 and 2015, respectively. He was a recipient of the National Graduate Student Scholarship in 2012, 2013, and 2014 from the Ministry of Education, China. Since 2017, he has served as an Associate Editor for both the IEEE Access and *Electronics Letters*. He has also served as an Editorial Board Member for both the *AEÜ-International Journal of Electronics and Communications* and *MDPI Electronics*.

Francisco Falcone (M'05, SM'09) received the degree in telecommunication engineering and the Ph.D. degree in communication engineering from the Universidad Pública de Navarra (UPNA), Spain, in 1999 and 2005, respectively. From February 1999 to April 2000, he was the Microwave Commissioning Engineer at Siemens-Italtel, deploying microwave access systems. From May 2000 to December 2008, he was a Radio Access Engineer at Telefónica Móviles, performing radio network planning and optimization tasks in mobile network deployment. In January 2009, as a co-founding member, he has been the Director of Tafco Metawireless, a spin-off company from UPNA, until May 2009. In parallel, he is an Assistant Lecturer with the Electrical and Electronic Engineering Department, UPNA, from February 2003 to May 2009. In June 2009, he becomes an Associate Professor with the EE Department, being the Department Head, from January 2012 to July 2018. From January 2018 to May 2018, he was a Visiting Professor with the Kuwait College of Science and Technology, Kuwait. He is also affiliated with the Institute for Smart Cities (ISC), UPNA, which hosts around 140 researchers. He is currently acting as the Head of the ICT Section. His research interests are related to computational electromagnetics applied to the analysis of complex electromagnetic scenarios, with a focus on the analysis, design, and implementation of heterogeneous wireless networks to enable context-aware environments. He has over 500 contributions in indexed international journals, book chapters, and conference contributions. He has been awarded the CST 2003 and CST 2005 Best Paper Award, the Ph.D. Award from the Colegio Oficial de Ingenieros de Telecomunicación (COIT), in 2006, the Doctoral Award UPNA, 2010, 1st Juan Gomez Peñalver Research Award from the Royal Academy of Engineering of Spain, in 2010, the XII Talgo Innovation Award 2012, the IEEE 2014 Best Paper Award, 2014, the ECSA-3 Best Paper Award, 2016, and the ECSA-4 Best Paper Award, 2017.